BIOCHEMISTRY
including biophysical chemistry & molecular biology

Article

pubs.acs.org/biochemistry

Interactions of Intermediate Semiquinone with Surrounding Protein Residues at the Q_H Site of Wild-Type and D75H Mutant Cytochrome bo_3 from *Escherichia coli*

Myat T. Lin,[†,@] Amgalanbaatar Baldansuren,[§] Richard Hart,[⊥] Rimma I. Samoilova,[∥] Kuppala V. Narasimhulu,[§] Lai Lai Yap,[‡] Sylvia K. Choi,[†] Patrick J. O'Malley,*[,⊥] Robert B. Gennis,*[,†,‡] and Sergei A. Dikanov*[,§]

[†]Center for Biophysics and Computational Biology, University of Illinois at Urbana-Champaign, Urbana, Illinois 61801, United States
[‡]Department of Biochemistry, University of Illinois at Urbana-Champaign, Urbana, Illinois 61801, United States
[§]Department of Veterinary Clinical Medicine, University of Illinois at Urbana-Champaign, Urbana, Illinois 61801, United States
[∥]Institute of Chemical Kinetics and Combustion, Russian Academy of Sciences, Novosibirsk 630090, Russia
[⊥]School of Chemistry, The University of Manchester, Manchester M13 9PL, U.K.

Supporting Information

ABSTRACT: Selective ^{15}N isotope labeling of the cytochrome bo_3 ubiquinol oxidase from *Escherichia coli* with auxotrophs was used to characterize the hyperfine couplings with the side-chain nitrogens from residues R71, H98, and Q101 and peptide nitrogens from residues R71 and H98 around the semiquinone (SQ) at the high-affinity Q_H site. The two-dimensional ESEEM (HYSCORE) data have directly identified N_ε of R71 as an H-bond donor carrying the largest amount of unpaired spin density. In addition, weaker hyperfine couplings with the side-chain nitrogens from all residues around the SQ were determined. These hyperfine couplings reflect a distribution of the unpaired spin density over the protein in the SQ state of the Q_H site and the strength of interaction with different residues. The approach was extended to the virtually inactive D75H mutant, where the intermediate SQ is also stabilized. We found that N_ε of a histidine residue, presumably H75, carries most of the unpaired spin density instead of N_ε of R71, as in wild-type bo_3. However, the detailed characterization of the weakly coupled ^{15}N atoms from selective labeling of R71 and Q101 in D75H was precluded by overlap of the ^{15}N lines with the much stronger ~1.6 MHz line from the quadrupole triplet of the strongly coupled $^{14}N_\varepsilon$ atom of H75. Therefore, a reverse labeling approach, in which the enzyme was uniformly labeled except for selected amino acid types, was applied to probe the contribution of R71 and Q101 to the ^{15}N signals. Such labeling has shown only weak coupling with all nitrogens of R71 and Q101. We utilize density functional theory-based calculations to model the available information about ^{1}H, ^{15}N, and ^{13}C hyperfine couplings for the Q_H site and to describe the protein−substrate interactions in both enzymes. In particular, we identify the factors responsible for the asymmetric distribution of the unpaired spin density and ponder the significance of this asymmetry to the quinone's electron transfer function.

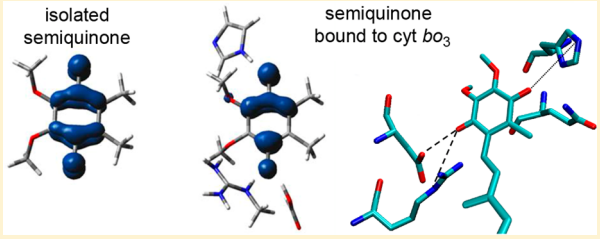

Cytochrome bo_3 ubiquinol oxidase (cyt bo_3) from *Escherichia coli* catalyzes the reduction of molecular oxygen to water using ubiquinol as the electron donor.[1] The enzyme located in the cytoplasmic membrane also functions as a proton pump, conserving much of the energy available from the redox reaction as the proton motive force.[2,3] Cyt bo_3 is a member of the heme-copper superfamily. Of the four subunits of cyt bo_3, the catalytic subunit and two other subunits are analogous to the mitochondrially encoded subunits of aa_3-type cytochrome *c* oxidase (cyt aa_3).[4] Despite having different electron donors, the proton pumps of cyt bo_3 and cyt aa_3 likely operate in a similar manner.[5]

Previous work has established that cyt bo_3 isolated in the detergent *n*-dodecyl β-D-maltoside (DDM) is associated with a tightly bound ubiquinone-8 (UQ_8) at the Q_H site, whereas purification in Triton X-100 yields the enzyme without any bound UQ_8.[6,7] The UQ_8 bound at the Q_H site does not exchange with the substrate ubiquinone pool during turnover. Hence, the Q_H site is distinct from the Q_L site, where the oxidation of substrate ubiquinol takes place.[7,8] The Q_H site has been shown to be able to stabilize the one-electron-reduced semiquinone (SQ_H), which can be detected by EPR spectroscopy.[9,10] The comparison of the kinetics between the enzyme preparations with and without the tightly bound UQ_8 or with the Q_H site inhibitors led to the conclusion that the UQ_8 at the

Received: February 2, 2012
Revised: April 11, 2012
Published: April 12, 2012

dx.doi.org/10.1021/bi300151q | *Biochemistry* 2012, 51, 3827−3838

Q_H site facilitates the fast electron transfer process from the substrate ubiquinol to low-spin heme *b*.[6,11−13]

A crystal structure of cyt bo_3 without a bound UQ_8 has been reported previously.[14] On the basis of the crystal structure and mutagenesis studies, residues R71, D75, H98, and Q101 from subunit I were proposed to interact with the bound UQ_8 at the Q_H site (Figure 1).[14,15] Mutating any of the four residues led to the loss of catalytic activity. Notably, the D75H mutant, despite its inability to reduce molecular oxygen, was found to stabilize a SQ radical with a midpoint potential similar to that of the wild-type (WT) enzyme.[15] Hence, an environment resulting in the stabilization of the SQ radical is necessary but not sufficient for proper function. A precise spatial arrangement of the SQ radical and the surrounding residues at the Q_H site is crucial for the successful electron transfer process.

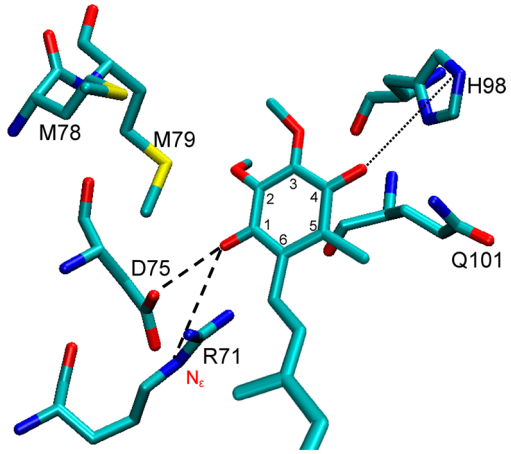

Figure 1. Current model of UQ at the Q_H site of cyt bo_3. The strong H-bonds are shown as dashed lines, and the weak one is shown as a dotted line. This figure was generated according to the model based on the X-ray crystal structure of Abramson et al.[14] Adapted from ref 20.

Previous X-band one-dimensional (1D) and two-dimensional (2D) ESEEM experiments have offered insights into the nature of interactions between the SQ_H and Q_H site residues (Figure 1).[16−20] Hyperfine couplings with methyl group protons and exchangeable, hydrogen-bonded protons are consistent with a neutral SQ_H species in WT cyt bo_3, indicating significant asymmetry in the distribution of the unpaired spin density.[17] The ^{14}N ESEEM spectra reveal one strongly coupled nitrogen participating in a hydrogen bond with the SQ_H.[16−18] In a previous work, we reported selective ^{15}N labeling of cyt bo_3, identifying N_ε of R71 as the strongly coupled nitrogen in WT cyt bo_3, and have shown that the other nitrogens of R71, H98, and Q101 possess substantially smaller couplings.[19] In contrast, a strongly coupled nitrogen that is observed in the ^{14}N ESEEM spectra of the SQ_H radical of the inactive D75H mutant was shown to be from a different amino acid residue.[18] The SQ_H is stabilized by hydrogen bonds different from those identified with the WT enzyme, and its characteristics are shifted toward those of an anion radical.

In the work presented here, we provide a comparative analysis of the 2D ESEEM (HYSCORE) spectra of ^{15}N uniformly labeled (^{15}N-U) WT and D75H cyt bo_3. We report the complete results of selective ^{15}N labeling of the residues at the Q_H site in these two enzymes. In addition to the strongly coupled N_ε atom of R71, the weakly coupled N_ε atom of H98 was also found to carry unpaired spin density in WT cyt bo_3. It is also shown that in the D75H mutant, N_ε of H75 is the strongly coupled nitrogen and N_ε of R71 displays significantly weaker hyperfine interaction with the SQ_H. The principal values of the rhombic hyperfine tensors for the strongly coupled nitrogens in WT and D75H cyt bo_3 were determined using a newly developed method of HYSCORE cross-peak line shape analysis. In addition to ^{15}N couplings from this work, ^{1}H and ^{13}C couplings from previous studies of WT and D75H cyt bo_3[17,18,20] were utilized in density functional calculations to calculate the spatial environment and electronic structure of the SQ_H. In particular, these calculations identify the factors responsible for the asymmetric distribution of the unpaired spin density and charge at the Q_H site and suggest the significance of this asymmetry to the quinone's electron transfer function.

MATERIALS AND METHODS

Materials. Isopropyl β-D-thiogalactopyranoside (IPTG) was from Fisher Scientific (Pittsburgh, PA). *n*-Dodecyl β-D-maltoside (DDM) was from Anatrace (Maumee, OH). $^{15}NH_4Cl$ and ^{15}N-enriched amino acids for the growth of *E. coli* for expressing isotope-labeled cyt bo_3 were ordered from Cambridge Isotope Laboratories (Andover, MA). Other chemicals used in the preparation of growth medium and buffers were from Sigma-Aldrich (St. Louis, MO).

Bacterial Strains. *E. coli* C43(DE3) strains with deletions of genes involved in amino acid biosynthetic pathways were constructed with the λ-Red recombination system as described previously.[20,21] The C43(DE3) auxotroph strains used in this work are listed in Table 1.

Preparation of Amino Acid Selective Isotope-Labeled Cyt bo_3. Selectively ^{15}N labeled cyt bo_3 samples were expressed from the various C43(DE3) auxotroph strains as summarized in Table 1. Each auxotroph to be used as an expression host was transformed with the pET-17b vector (Novagen) encoding the WT or D75H mutant *cyo* operon engineered to encode cyt bo_3 with a six-His tag at the C-terminus of subunit II.[18] The enzymes overexpressed from the C43(DE3) cultures were solublized in DDM detergent, purified via Ni-NTA affinity chromatography, and reduced with sodium ascorbate under anaerobic conditions to generate the SQ_H radical as described previously.[20]

EPR Measurements. The CW EPR measurements were performed on an X-band Varian EPR-E122 spectrometer. The pulsed EPR experiments were conducted using an X-band Bruker ELEXSYS E580 spectrometer equipped with Oxford CF 935 cryostats. Unless otherwise indicated, all measurements were taken at 50 K. Some pulsed EPR measurements were also performed at higher temperatures, up to 120 K, and the results were similar to those obtained at 50 K. Several types of ESE experiments with different pulse sequences were employed with appropriate phase cycling schemes to eliminate unwanted features from the experimental echo envelopes. Among them are two-dimensional three-pulse and four-pulse sequences, which are described in detail elsewhere.[17] Spectral processing of three- and four-pulse ESEEM patterns, including subtraction of the relaxation decay (fitting by third- to sixth-order polynomials), apodization (Hamming window), zero filling, and fast Fourier transformation, was performed using Bruker WIN-EPR software.

Some HYSCORE spectra are presented as contour plots in Matlab R14. For the representation of 2D data, the echo decay was eliminated by low-order polynomial (up to fourth-order)

Table 1. Genotypes of *E. coli* C43(DE3) Auxotrophs Used for the Preparation of Selectively ^{15}N-Labeled Cyt bo_3 Samples and Amino Acids Added to the Minimal Medium for the Growth of These Auxotrophs

E. coli C43(DE3) strain	genes knocked out	amino acids added to the minimal medium	cyt bo_3 samples prepared
C43(DE3)	none	none	uniformly ^{15}N-labeled WT cyt bo_3
CLY	*cyo*	none	uniformly ^{15}N-labeled D75H cyt bo_3
ML8	*cyo, argH*	105 mg/L Arg	(1) WT cyt bo_3 with $^{15}N_\eta$ of Arg, (2) WT cyt bo_3 with $^{15}N_\alpha$ of Arg, (3) WT cyt bo_3 with $^{15}N_4$ of Arg, (4) D75H cyt bo_3 with uniform ^{15}N labeling except for Arg, (5) D75H cyt bo_3 with uniform ^{15}N labeling except for N_ε and N_α of Arg
ML17	*glnA*	750 mg/L Gln	WT cyt bo_3 with $^{15}N_\varepsilon$ of Gln
ML21	*tyrA, hisG*	18 mg/L Tyr, 15 mg/L His	(1) WT cyt bo_3 with $^{15}N_3$ of His, (2) WT cyt bo_3 with $^{15}N_\delta$ of His
ML22	*cyo, ilvE, avtA, aspC, hisG*	40 mg/L Ile, 40 mg/L Leu, 35 mg/L Val, 90 mg/L Tyr, 50 mg/L Phe, 40 mg/L Asp, 16 mg/L His	(1) WT cyt bo_3 with ring $^{15}N_2$ of His, (2) D75H cyt bo_3 with $^{15}N_3$ of His, (3) D75H cyt bo_3 with $^{15}N_\delta$ of His
ML26	*cyo, ilvE, avtA, aspC, hisG, argH*	40 mg/L Ile, 40 mg/L Leu, 35 mg/L Val, 90 mg/L Tyr, 50 mg/L Phe, 40 mg/L Asp, 16 mg/L His, 105 mg/L Arg	D75H cyt bo_3 with $^{15}N_4$ of Arg
ML30	*cyo, ilvE, avtA, aspC, hisG, argH, glnA*	40 mg/L Ile, 40 mg/L Leu, 35 mg/L Val, 90 mg/L Tyr, 50 mg/L Phe, 40 mg/L Asp, 16 mg/L His, 105 mg/L Arg, 750 mg/L Gln	D75H cyt bo_3 with $^{15}N_\varepsilon$ of Gln
ML32	*cyo, argH, glnA*	105 mg/L Arg, 750 mg/L Gln	D75H cyt bo_3 with uniform ^{15}N labeling except for Arg and Gln
ML34	*cyo, argH, glnA, hisG*	105 mg/L Arg, 750 mg/L Gln, 16 mg/L His	WT cyt bo_3 with uniform ^{15}N labeling except for Arg, Gln, and His

baseline corrections in each dimension and apodized with a Hamming window subsequently. Before the 2D Fourier transformation, the data were zero-filled up to a 1024 × 1024 matrix. The evaluated values were subsequently used to simulate the 2D HYSCORE spectra applying the Kazan Viewer package[22] or home-written software developed by A. Tyryshkin (now at Princeton University, Princeton, NJ).[23]

HYSCORE Spectra from ^{15}N Nuclei. The experimental data regarding the ligand environment of the semiquinone were obtained in this work from 2D ^{15}N ESEEM (HYSCORE) spectra.[24] The HYSCORE technique creates 2D spectra with off-diagonal cross-peaks. An $I = {}^1/_2$ ^{15}N nucleus has two hyperfine frequencies, ν_α and ν_β, from opposite $m_s = \pm{}^1/_2$ electron spin manifolds. These may produce a pair of cross-features (ν_α, ν_β) and (ν_β, ν_α) in the (++) quadrant, as well as another pair ($-\nu_\alpha$, ν_β) and (ν_α, $-\nu_\beta$) in the (+−) quadrant. The appearance of cross-peaks in (++) or (+−) quadrants is governed by the relative values of hyperfine couplings ^{15}A and the Zeeman frequency $^{15}\nu_N$.[25,26] Peaks in the (+−) quadrant come primarily from strong hyperfine interaction, i.e., $|^{15}A| > 2(^{15}\nu_N)$, whereas peaks in the (++) quadrant appear predominantly from interactions for which $|^{15}A| < 2(^{15}\nu_N)$. Peaks may appear in both quadrants simultaneously in the intermediate case when both parts of the inequalities are comparable.

Orientation-disordered (i.e., powder) 2D spectra of $I = {}^1/_2$ nuclei also reveal, in the form of cross-ridge contour projections, the interdependence between values of ν_α and ν_β in the same orientation. The two coordinates of the arbitrary point at the cross-ridge, described in the first order by equation

$$\nu_{\alpha(\beta)} = |^{15}\nu_N \pm |^{15}A|/2| \quad (1)$$

can be used for the first-order estimate of the corresponding hyperfine coupling constant A:

$$\nu_\alpha - \nu_\beta = |A| \text{ if } |^{15}A| < 2(^{15}\nu_N) \quad (2)$$

$$\nu_\alpha + \nu_\beta = |A| \text{ if } |^{15}A| > 2(^{15}\nu_N)$$

On the other hand, analysis of the cross-ridges in $(\nu_\alpha)^2$ versus $(\nu_\beta)^2$ coordinates and spectral simulations allows in many cases for simultaneous determination of the isotropic a_{iso} and anisotropic T components of the hyperfine tensor.[25,26]

Computational Methods. All density functional calculations were performed using Gaussian 09.[27] All calculations, including geometry optimization and hyperfine coupling, were performed using the B3LYP functional and the EPR-II basis set. Specific details concerning hyperfine coupling calculations are as previously described.[28,29] Details of specific models used are given in the text.

RESULTS AND DISCUSSION

^{14}N and ^{15}N ESEEM Spectra of Wild-Type and D75H Mutant Cyt bo_3. The interaction of the SQ_H with the protein environment in WT and D75H cyt bo_3 with a natural abundance of nitrogen (^{14}N isotope, 99.63%) has been previously studied in detail by pulsed EPR spectroscopy.[16−18] 1D and 2D ^{14}N ESEEM spectra show the contribution from only a single nitrogen in each protein (Figures S1 and S2 of the Supporting Information). These possess different characteristics, i.e., quadrupole coupling constant (qcc) K = 0.93 MHz, asymmetry parameter η = 0.51, and hyperfine coupling ^{14}A = 1.8 MHz for WT cyt bo_3[16,17] and K = 0.43 MHz, η = 0.73, and

dx.doi.org/10.1021/bi300151q | *Biochemistry* 2012, 51, 3827−3838

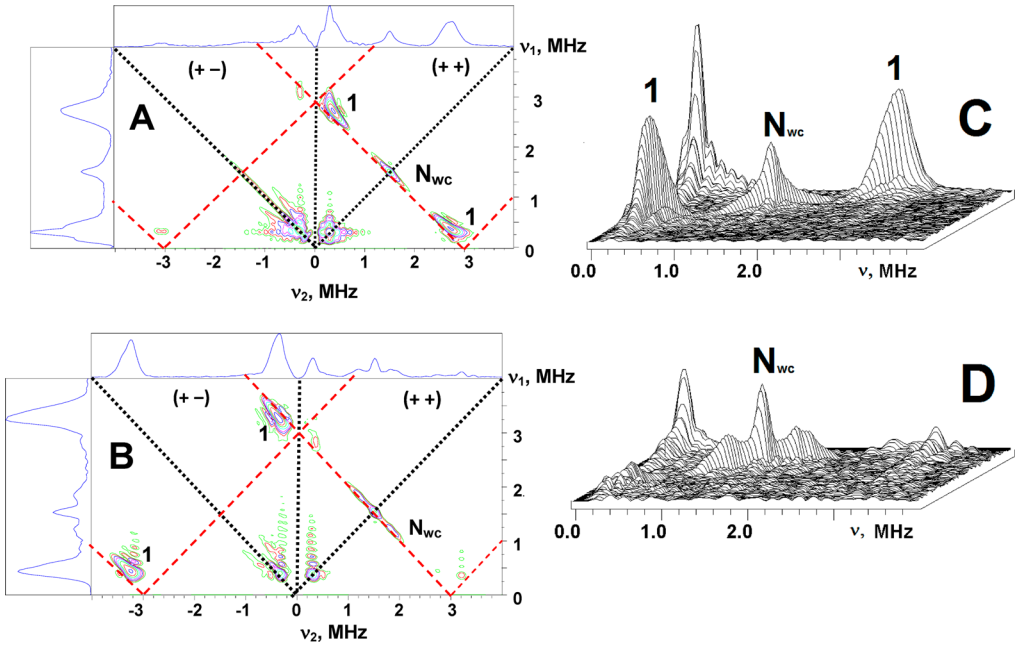

Figure 2. (A and B) Contour presentation of the ^{15}N HYSCORE spectra of the SQ_H in uniformly ^{15}N-labeled WT (A) and D75H (B) cyt bo_3 [magnetic field of 345.2 (A) or 346.1 mT (B), time between first and second pulses (τ) of 136 ns, microwave frequency of 9.702 (A) or 9.704 GHz (B)]. (C and D) Stacked presentation of the (++) quadrant of the WT (C) and D75H (D) spectra. Stacked presentation of the full (A and B) spectra is shown in Figure S4 of the Supporting Information. Red dashed line segments are defined by $|\nu_1 \pm \nu_2| = 2(^{15}\nu_N)$.

^{14}A = 2.7 MHz for D75H.[18] The values of K and η characterize the chemical type and electronic configuration of the ^{14}N atom interacting with the SQ_H. For instance, the relationship $K = e^2qQ/4h$ = 0.93 MHz most closely corresponds to the nitrogen from an NH or NH_2 group.[17,18] This value is ∼10% larger than the qcc for the peptide amide nitrogen and more than 2 times the qcc of the protonated imidazole nitrogens in histidine. Therefore, it was suggested that the most likely candidates for the H-bond donor in WT cyt bo_3 are the nitrogens from the side chains of R71 or Q101. Likewise, a protonated imidazole nitrogen of H75 or H98 was suggested as the H-bond donor in the D75H mutant.[18] ^{14}N spectra do not show any lines from other side-chain and peptide nitrogens of the nearby environment. These nitrogens are coupled more weakly and do not produce well-defined lines in the ^{14}N powder-type spectra, because of the influence of the nuclear quadrupole interaction (nqi).[30,31] In contrast, the lines from weakly coupled nitrogens ($\mathbf{N_{wc}}$) are well observed in 2D ^{15}N ESEEM spectra, which are not complicated by nqi.

Two presentations of the ^{15}N HYSCORE spectrum of the SQ_H in ^{15}N-U WT cyt bo_3 are shown in panels A and C of Figure 2 (see also Figure S3 of the Supporting Information). The (++) quadrant exhibits a pair of intensive cross-peaks **1** located symmetrically around the diagonal point ($^{15}\nu_N$, $^{15}\nu_N$), along the antidiagonal with maxima at (2.74, 0.34) MHz, which correspond to a hyperfine coupling ^{15}A of 2.4 MHz. This coupling is in agreement with the expected ^{15}A of 2.5 MHz rescaled from the hyperfine coupling ^{14}A of 1.8 MHz measured from ^{14}N ESEEM spectra. In addition, the (++) quadrant contains feature $\mathbf{N_{wc}}$ with the maximum near the diagonal point ($^{15}\nu_N$, $^{15}\nu_N$) with the decaying shoulders symmetrically extended up to ∼0.8 MHz along the antidiagonal.

The ^{15}N HYSCORE spectrum of the ^{15}N-U D75H mutant (Figure 2B,D) shows a pair of intensive cross-peaks **1** in the (+−) quadrant with maxima at ∼(±3.3, ∓0.4) MHz defining ^{15}A = 3.7 MHz or ^{14}A = 2.6 MHz, also consistent with the coupling estimated from ^{14}N spectra. The (++) quadrant of the spectrum (Figure 2B,D) also exhibits a $\mathbf{N_{wc}}$ feature located around the ($^{15}\nu_N$, $^{15}\nu_N$) point. The $\mathbf{N_{wc}}$ feature in D75H has a different shape compared to that of the WT enzyme. For D75H, the $\mathbf{N_{wc}}$ feature is a triplet, including a central peak at ($^{15}\nu_N$, $^{15}\nu_N$) and two other lines symmetrically located around the antidiagonal with a splitting of ∼0.6 MHz.

The ^{14}N and ^{15}N ESEEM spectra show the presence of one strongly coupled nitrogen in the SQ_H environment, which is different in the WT and D75H cyt bo_3 proteins. In contrast, the $\mathbf{N_{wc}}$ features resolved in ^{15}N spectra of both the WT and D75H mutant result from multiple nonequivalent contributions of weakly coupled nitrogen nuclei in the immediate vicinity of the SQ_H. The shapes of the $\mathbf{N_{wc}}$ features indicate differences in the individual interactions for the SQ_H of the WT and D75H mutant. To further resolve the interactions with nitrogens in the SQ_H environment, we employed selective ^{15}N labeling of different residues, as well as ^{15}N uniform labeling.

Selective ^{15}N Labeling of WT Cyt bo_3. Arg, His, and Gln were targeted for selective ^{15}N labeling because the corresponding residues are involved in the current model of the Q_H site (Figure 1). The molecular structure and atomic numbering of each of the three amino acids are displayed in Figure S4 of the Supporting Information. The following samples of WT cyt bo_3 were prepared with ^{15}N labels as follows. (1) Arg, (a) uniform labeling, (b) the two N_η positions, and (c) peptide position N_α; (2) His, (a) uniform labeling, (b) ring ^{15}N (N_δ and N_ε), and (c) the N_δ position only; (3) Gln with ^{15}N in the N_ε position; and (4) uniformly labeled with ^{15}N except for Arg, Gln, and His. It is assumed that only R71, Q101, and H98 are significant in the interpretation of the interactions with SQ_H.

The following results were obtained.

dx.doi.org/10.1021/bi300151q | Biochemistry 2012, 51, 3827−3838

(1) As shown previously, a dramatic change of the ESEEM spectra, accompanied by the complete disappearance of the ^{14}N peaks, is observed with WT cyt bo_3 with uniformly ^{15}N-labeled R71 (ref 19 and Figure S5A of the Supporting Information). The HYSCORE spectrum of the SQ_H in this protein contains two intense cross-peaks **1** similar to those in the spectrum of ^{15}N-U WT cyt bo_3 (Figure 2A,C). In contrast, the $\mathbf{N_{wc}}$ feature observed with ^{15}N-U R71 WT cyt bo_3 is very different (Figure S5A of the Supporting Information) and resolves only a weak doublet centered around the ($^{15}\nu_N$, $^{15}\nu_N$) diagonal point with the splitting $^{15}A = 0.15$ MHz. A similar doublet was observed in the spectrum of WT cyt bo_3 with the selectively labeled $^{15}N_\eta$ positions in R71 (ref 19 and Figure S5B of the Supporting Information), whereas no ^{15}N-resolved peaks were observed in a sample in which the peptide N_α of R71 was selectively labeled with ^{15}N. These observations show a weak interaction in WT cyt bo_3 between the SQ_H and $^{15}N_\eta$ of R71 and confirm that N_ε of R71 possesses the largest hyperfine coupling and is responsible for the ^{14}N spectral features of WT cyt bo_3.

(2) It was previously shown that the spectrum of cyt bo_3 with uniformly ^{15}N-labeled H98 shows the $\mathbf{N_{wc}}$ feature with a maximum at the ($^{15}\nu_N$, $^{15}\nu_N$) point accompanied by extended shoulders up to 0.6 MHz with very poorly resolved maxima.[19] This line can be produced by the interactions with up to three ^{15}N atoms, and additional selective ^{15}N labeling was performed to clarify the origins of this feature. The spectra of the sample with ring ^{15}N (N_δ and N_ε)-labeled His is identical to that with uniformly ^{15}N-labeled His (Figure S5C,D of the Supporting Information), but a very week antidiagonal ^{15}N line is found in the spectrum of the protein with $^{15}N_\delta$ of His. Thus, it is concluded that the extended $\mathbf{^{15}N_{wc}}$ feature is primarily due to N_ε of H98.

It is noted that a peak of very low intensity located at the diagonal point ($^{15}\nu_N$, $^{15}\nu_N$) was previously observed for WT cyt bo_3 with a ^{15}N-labeled N_ε of Q101, indicating very weak dipolar interaction between the unpaired electron and a distant ^{15}N nucleus.[19] No ^{15}N signal was found in the spectra of WT cyt bo_3 uniformly labeled with ^{15}N except for Arg, Gln, and His. On the basis of these observations, we conclude that the only contributions to the $\mathbf{N_{wc}}$ feature are from R71, Q101, and H98.

Selective ^{15}N Labeling of D75H. Selectively ^{15}N labeled D75H cyt bo_3 samples were also examined. The ^{14}N signals completely disappeared in the HYSCORE spectrum of D75H with uniformly $^{15}N(3)$-labeled His (Figure S6 of the Supporting Information). This result is consistent with the prediction, based on the value of the qcc, that the ^{14}N ESEEM spectrum of the D75H mutant arises from the protonated imidazole ring nitrogen of a histidine residue, presumably either H75 or H98.[18] To definitively identify whether N_δ or N_ε of His contributes to the ^{14}N ESEEM spectra, a D75H mutant with $^{15}N_\delta$ of His was prepared. The ^{14}N HYSCORE spectrum of this sample is identical to the spectrum of unlabeled D75H in Figure S2 of the Supporting Information, so we can conclude that these spectroscopic features originate from the N_ε atom of a His residue.

The $\mathbf{N_{wc}}$ feature in the HYSCORE spectrum from the enzyme with uniformly labeled $^{15}N(3)$ His possesses the maximal intensity at the ($^{15}\nu_N$, $^{15}\nu_N$) diagonal point and shoulders extended up to 0.5 MHz in both directions from the diagonal (Figure 3B). However, the total intensity of the diagonal peak and shoulders is substantially lower than in the ^{15}N-U enzyme (Figure 3A), using the cross-peaks **1** as the reference for the intensity comparison. The larger intensity and different shape of the $\mathbf{N_{wc}}$ feature that is observed only in the uniformly labeled ^{15}N-U D75H mutant must be due to the additional contributions from nitrogens in R71 and Q101.

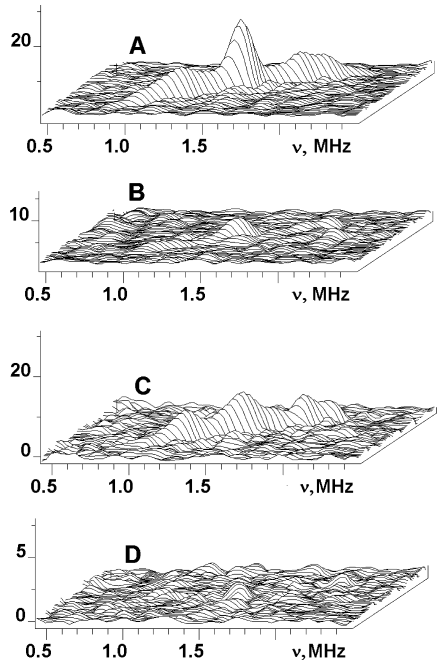

Figure 3. $\mathbf{N_{wc}}$ feature in ^{15}N HYSCORE spectra of the SQ_H in ^{15}N-U D75H (A), in D75H with uniformly $^{15}N(3)$-labeled His (B), (C) obtained as a difference between the spectra of ^{15}N-U D75H and ^{15}N-U D75H except Arg, and (D) obtained as a difference between the spectra of ^{15}N-U D75H except Arg and D75H with uniformly $^{15}N(3)$-labeled His.

Unfortunately, the HYSCORE spectra recorded for D75H selectively labeled with ^{15}N-labeled Arg or ^{15}N-labeled Gln do not resolve the signals from the weakly coupled ^{15}N because any such signal is overshadowed by a much more intense peak $\nu_+ = 1.61$ MHz from the strongly coupled $^{14}N_\varepsilon$ atom of His (Figure S7 of the Supporting Information). To visualize the $\mathbf{N_{wc}}$ from R71 and Q101 in the D75H mutant, a reverse labeling approach was employed to prepare ^{15}N-U D75H except for Arg. The contributions of the nitrogen interactions from R71 and Q101 to the ^{15}N spectrum were then obtained using the spectra of (a) ^{15}N-U D75H, (b) D75H with ^{15}N-His(3), and (c) ^{15}N-U D75H with ^{14}N-labeled Arg. The subtractions of a minus c and c minus b give the $\mathbf{^{15}N_{wc}}$ difference spectra from R71 and Q101, respectively (Figure 3C,D). The difference spectrum isolating the contribution from R71 shows extended shoulders with the maximum corresponding to a splitting of ~0.6 MHz. The difference spectrum showing the contribution from Q101 consists of a weak peak at the diagonal point ($^{15}\nu_N$, $^{15}\nu_N$). In addition, we have prepared ^{15}N-U D75H except for the N_ε and N_α atoms of Arg. The shape of $\mathbf{N_{wc}}$ for this sample is similar to that of D75H with ^{15}N-His(3). This result indicates that the cross-peaks with a splitting of 0.6 MHz are produced by N_ε of R71 that forms an H-bond with the SQ_H in D75H as well.

In contrast to WT cyt bo_3, there are two histidines, i.e., H75 and H98, around the SQ_H in the D75H mutant. Experimental $^{14,15}N$ spectra do not give any indication about which of them carries the greatest spin density on the N_ε atom. However, in our previous work, we have provided arguments based on the

dx.doi.org/10.1021/bi300151q | Biochemistry 2012, 51, 3827−3838

comparison of the hyperfine couplings with methyl protons reflecting asymmetry in spin density distribution with the Q_A site SQ of the reaction center that stronger interaction with N_ε of H75 is more preferable.[18] Taking into account this assignment, one can conclude that the $\mathbf{N_{wc}}$ pattern in D75H with ^{15}N-His(3) includes contributions from N_δ of H75 and N_δ and N_ε of H98. The $\mathbf{N_{wc}}$ shoulders in this sample (Figure 3B) show a slight increase of intensity corresponding to a splitting of ~0.8 ± 0.2 MHz. We suggested that N_ε from H98 forms an H-bond with the SQ_H as with WT cyt bo_3 and produces this splitting. The N_δ atoms of H75 and H98 separated by two bonds from H-bonded N_ε atoms would have much smaller couplings and would contribute to the central part of the $\mathbf{N_{wc}}$ line around the diagonal point. This suggestion is supported by an ~1/20 ratio of the hyperfine couplings for the remote and coordinated imidazole nitrogens in complexes with metals and clusters.[32] We also suggested that N_α atoms from both His residues have a negligible influence on the spectra as in the WT protein.

Hyperfine Tensors of Strongly Coupled Nitrogens. So far in our description of the experimental spectra, we have used the hyperfine couplings determined from the position of cross-peak maxima using first-order expressions for two nuclear frequencies (eqs 1 and 2) of ^{15}N nuclei. However, the line shape of the cross-peaks from strongly coupled nitrogens in WT and D75H cyt bo_3 allows one to determine all of the principal values of hyperfine tensors. The cross-peaks from these nuclei possess the hornlike line shape that indicates a significant rhombicity of the corresponding hyperfine tensors.[25,26] The principal values of the rhombic hyperfine tensor can be defined as follows: $A_x = a_{iso} - T(1 + \delta)$, $A_y = a_{iso} - T(1 - \delta)$, $A_z = a_{iso} + 2T$ with $0 \le \delta \le 1$, where a_{iso} and T are the isotropic and anisotropic components of hyperfine coupling, respectively, and δ is a rhombic parameter. The two nuclear frequencies of ^{15}N ($I = {}^1/_2$) from opposite $m_s = \pm{}^1/_2$ electron spin manifolds for each principal value $i = x, y, z$ are as follows: $\nu_{\alpha i} = |{}^{15}\nu_N + |A_i|/2|$, and $\nu_{\beta i} = |{}^{15}\nu_N - |A_i|/2|$. An estimate of the principal components can be performed using theoretical predictions of the line shape of the cross-peaks in powder-type spectra. The borders of the ideal cross-peak horn in such spectra are formed by three arc-type ridges among the pairs of three points ($\nu_{\alpha x}$, $\nu_{\beta x}$), ($\nu_{\alpha y}$, $\nu_{\beta y}$), and ($\nu_{\alpha z}$, $\nu_{\beta z}$) located on the $|\nu_1 \pm \nu_2| = 2({}^{15}\nu_N)$ lines. The shape of these ridges is described by the general equation (where Q and G are coefficients that are functions of a_{iso}, T, δ, and $^{15}\nu_N$):[25,26]

$$\nu_\alpha{}^2 = Q\nu_\beta{}^2 + G \qquad (3)$$

The arc-type ridges transform to straight segments in $(\nu_1)^2$ versus $(\nu_2)^2$ plots, producing a triangle line shape of the cross-peak with triangle vertices at $((\nu_{\alpha(\beta)x})^2, (\nu_{\beta(\alpha)x})^2)$, $((\nu_{\alpha(\beta)y})^2, (\nu_{\beta(\alpha)y})^2)$, and $((\nu_{\alpha(\beta)z})^2, (\nu_{\beta(\alpha)z})^2)$.[25] It should be noted that HYSCORE intensity at ($\nu_{\alpha x}$, $\nu_{\beta x}$), ($\nu_{\alpha y}$, $\nu_{\beta y}$), and ($\nu_{\alpha z}$, $\nu_{\beta z}$) points corresponding to orientations of magnetic field along the principal directions (x, y, z) of the hyperfine tensor is equal to zero and significantly suppressed in the orientations around principal directions.[26] Therefore, in HYSCORE spectra, only the central part of the border cross-ridges, which correspond to orientations of the magnetic field substantially different from the principal directions, will possess substantial intensity.[26] It means that in the real spectrum the cross-peak borders should not cross the $|\nu_1 \pm \nu_2| = 2({}^{15}\nu_N)$ line(s) and the crossing points ($\nu_{\alpha x}$, $\nu_{\beta x}$), ($\nu_{\alpha y}$, $\nu_{\beta y}$), and ($\nu_{\alpha z}$, $\nu_{\beta z}$) can be obtained through the linear regression of the observed parts of border arcs in the $(\nu_1)^2$ versus $(\nu_2)^2$ presentation of the spectrum.

Figure 4 (top) shows a presentation of the (++) quadrant of the ^{15}N HYSCORE spectrum of the SQ_H in WT cyt bo_3 in

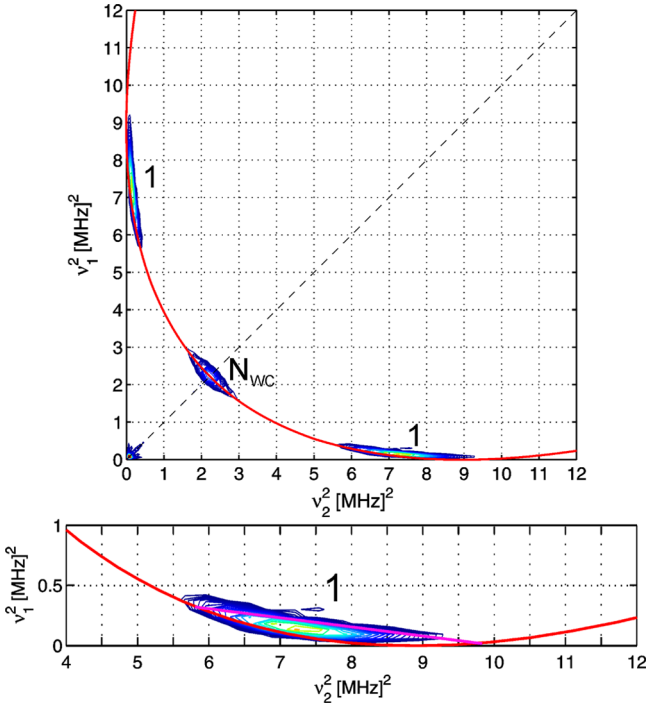

Figure 4. Contour presentation (top) of the (++) quadrant from the ^{15}N HYSCORE spectrum of the SQ_H in uniformly ^{15}N-labeled WT cyt bo_3 (Figure 2A) in $(\nu_1)^2$ vs $(\nu_2)^2$ coordinates. The red curve is defined by $|\nu_1 \pm \nu_2| = 2({}^{15}\nu_N)$. Analysis of the cross-peak **1** contour line shape (bottom). Linear regression of the border segment (pink line) gives two crossing points ($(\nu_{\beta x})^2$, $(\nu_{\alpha x})^2$) and ($(\nu_{\beta z})^2$, $(\nu_{\alpha z})^2$) with the $|\nu_1 \pm \nu_2| = 2({}^{15}\nu_N)$ curve corresponding to minimal and maximal principal values of the hyperfine tensor.

$(\nu_1)^2$ versus $(\nu_2)^2$ coordinates. The borders of the cross-peaks can be estimated by the area of the sharp increase in peak intensity, i.e., where the blue background transformed into the colored area in Figure 4. In the spectrum shown in Figure 4 (bottom), only one border segment with a well-defined linear portion can be defined (pink line segment). Linear regression of this segment (pink line in Figure 4, bottom) gives two crossing points ($(\nu_{\beta x})^2$, $(\nu_{\alpha x})^2$) and ($(\nu_{\beta z})^2$, $(\nu_{\alpha z})^2$), corresponding to the minimal and maximal principal values. The larger coordinate of the crossing points is estimated by the values of 5.5−5.8 and 9.7−10.0 MHz^2 that define $\nu_{\alpha x}$ = 2.3−2.4 MHz or $|A_x|$ = 1.7 ± 0.1 MHz and $\nu_{\alpha z}$ = 3.1−3.2 MHz or $|A_z|$ = 3.3 ± 0.1 MHz, respectively. The intermediate principal value was determined from the simulations of ^{15}N HYSCORE spectra. Simulations varying the tensor anisotropy from axial (δ = 1) to completely rhombic (δ = 0) show that best agreement in the location of cross-peaks **1** (Figure S8 of the Supporting Information) was achieved with δ = 0.64 ± 0.05 and defines the complete hyperfine tensor as $|A_z|$ = 3.3 MHz, $|A_y|$ = 2.3 MHz, $|A_x|$ = 1.7 MHz (±0.1 MHz) with a_{iso} = 2.42 MHz and $\mathbf{T}$ = (0.88, −0.16, −0.72) MHz (signs of a and $\mathbf{T}$ components are relative). All principal values of A_i should have the same sign. Only this selection correctly describes the location of the cross-peak and gives the isotropic coupling consistent with the values estimated from ^{14}N and ^{15}N spectra. This tensor is assigned to

dx.doi.org/10.1021/bi300151q | Biochemistry 2012, 51, 3827−3838

N_ε of R71. A similar analysis was performed for cross-peaks **1** in the (+−) quadrant of the ^{15}N HYSCORE spectrum of the SQ_H in the D75H mutant (see Figures S9 and S10 of the Supporting Information). Determined principal values of the hyperfine tensor assigned to N_ε of H75 are listed in Table 2.

Table 2. Hyperfine Tensors of ^{15}N Nuclei at the Q_H Site of Cyt bo_3 Proteins

Cyt bo_3	residue	nitrogen	hyperfine tensors (MHz)
WT	R71	N_ε	a_{iso} = 2.42, **T** = (0.88, −0.16, −0.72)
		N_η	a_{iso} ∼ 0.15, T < 0.05−0.1
		N_α	∼0
	H98	N_δ	∼0
		N_ε	a_{iso} = 0.3, T ∼ 0.3−0.4
		N_α	∼0
	Q101	N_ε	weak dipolar coupling <0.05−0.1
D75H	H75	N_ε	a_{iso} = 3.5, **T** = (0.9, −0.2, −0.7)
	H98	N_ε	a_{iso} = 0.8, $\|T\|$ ∼ 0.3−0.4
		N_δ	
	R71	N_ε	a_{iso} = 0.6, $\|T\|$ ∼ 0.4−0.5
		N_η	∼0
	Q101	N_ε	weak dipolar coupling <0.05−0.1

Hyperfine Tensors of Other Nitrogens. In addition, simulations of the ^{15}N HYSCORE spectra were used to estimate the isotropic and anisotropic components of the hyperfine tensors for weakly coupled nitrogens, i.e., N_η of R71 and N_ε of H98 in WT cyt bo_3 and N_ε of H98 and N_ε of R71 in D75H cyt bo_3. The results of simulations are provided in Table 2. The $\mathbf{N_{wc}}$ spectra are extended along antidiagonal of the (++) quadrant. They possess a narrow line width in the direction normal to the antidiagonal and symmetrical line shapes with the cross-peak maximum corresponding to the undefined orientation of the magnetic field relative to the principal axes. The intensity is suppressed at the cross-peak wings corresponding to field orientations along or near the axes with maximal and minimal principal values of the tensor. Our previous analysis of the ^{15}N HYSCORE spectra[23] and simulations have shown that the position of the maximum gives an accurate estimate of the isotropic coupling (approximately ±0.05 MHz), but the relative signs of the isotropic and anisotropic components and symmetry of the tensor (i.e., axial or rhombic) are uncertain from the $\mathbf{N_{wc}}$ line shape. This uncertainty influences the accuracy in the anisotropic tensor estimate to a larger degree, i.e., for T values of ∼0.3−0.4 MHz, and the accuracy in its determination is ∼0.1−0.15 MHz.

Density Functional Studies. Previous modeling studies used water molecules and *N*-methylformamide groups as hydrogen bond donors to the O1 and O4 atoms of the SQ_H and did not take into account the varying strengths of hydrogen bond interactions with the SQ_H by different groups.[33−35] In our work, based on the X-ray structure, Figure 1, and the EPR and mutational data for the WT enzyme, the SQ_H was modeled to have hydrogen bonds to the OH group of the carboxylic acid group of D75, the $N_\varepsilon H$ group of the imidazole group of H98, and the $N_\varepsilon H$ group of the guanidinium group of R71. In the absence of accurate data from the X-ray crystal structure, we explored idealized small models with geometry optimization. Therefore, the overall significance and relative strength of each interaction can be assessed by the spin density distribution, but the correct orientation of the hydrogen bonds with the SQ_H will not be reproduced well.

Computed Geometries. Table 3 lists the calculated geometries of the isolated SQ_H and the effect of hydrogen bonding on this geometry in the WT and D75H models. For the WT model, the lengths of hydrogen bonds from O1 to the $N_\varepsilon H$ group of R71 (1.65 Å) and the carboxylic acid group of D75 (1.60 Å) are considerably shorter than those formed at O4 with the imidazole NH group representing H98 (1.83 Å). These bond distance trends suggest stronger hydrogen bonding to the O1 atom of the SQ_H caused principally by the strong interaction with the carboxylic acid group and the positively charged guanidinium group. The NH group of the H98 imidazole is a weaker hydrogen bond donor. For the D75H model, the length of the hydrogen bond to the imidazole NH group of H75 is also significantly longer (1.79 Å) than that found for the carboxylic acid group of D75 in the WT model (1.60 Å), suggesting a weaker hydrogen bond formed by the imidazole group in the mutant.

Table 3. Optimized Geometries with Distances in Angstroms

	isolated	WT	D75H
C1−O1	1.27	1.30	1.30
C4−O4	1.27	1.27	1.27
O1−H (R71)	–	1.65	1.61
O1−H (D75/H75)	–	1.60	1.79
O4−H (H98)	–	1.83	1.82

Spin Densities and Populations. Figure 5 shows the spin density distribution changes that occur on going from the isolated SQ to the WT and D75H models. Figure 6 provides a more quantitative picture using spin populations obtained from a Mulliken population analysis. The spin density distribution of the isolated SQ is symmetric, whereas in contrast, it is highly asymmetric for both the WT and D75H. For simpler semiquinone models, the primary effect of hydrogen bonding to either of the semiquinone carbonyl oxygen atoms is a redistribution of spin density from the oxygen atom position to the adjacent carbon.[36] In our WT model (Figure 6), the spin density redistribution is mainly from O1 to C1, with a much smaller redistribution occurring between C4 and O4. The charged guanidinium and carboxylic acid groups polarize the C1−O1 bond. The increased spin population at C1 leads via spin polarization to a lower spin population at positions C2 and C6 and a higher spin population at positions C3 and C5. This "domino" spin polarization effect should lead to a significantly lower spin population at C4, but this is offset by the presence of a hydrogen bond from the imidazole group of H98 to the O4 atom, which partially balances the spin polarization effect on C4. The spin populations obtained for the WT can, therefore, be explained by the presence of strong hydrogen bonds to the O1 atom of the SQ_H and a significantly weaker hydrogen bond to the O4 atom, in accord with EPR studies. For the D75H model, the spin populations are slightly less asymmetric than those of the WT model. As noted above, the hydrogen bond made by the imidazole is longer than that calculated for the carboxylic acid group, suggesting a weaker hydrogen bond is formed by this group. The predicted spin density distributions are also in accord with the lower 5-CH_3 ^1H and ^{13}C hyperfine couplings measured for the D75H mutant, as discussed below.

Comparison of Calculated and Experimental Hyperfine Couplings. In addition to the spin density distribution,

dx.doi.org/10.1021/bi300151q | *Biochemistry* 2012, 51, 3827−3838

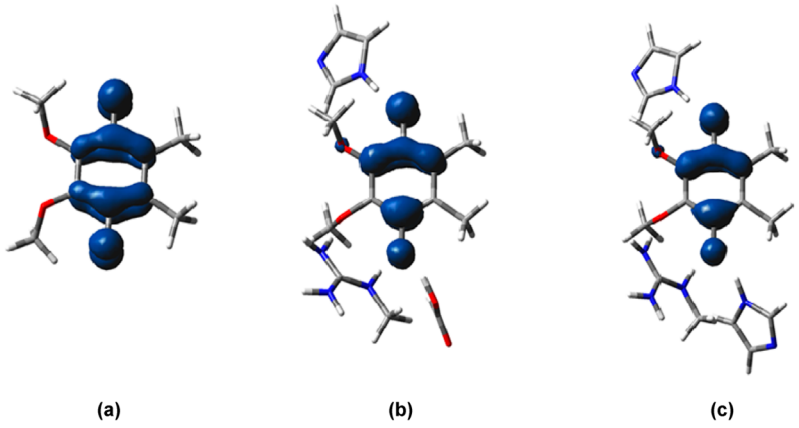

Figure 5. Spin density contour plots (0.004 e/au) for (a) isolated, (b) WT, and (c) D75H models. Atom numbering is as shown in Figure 1.

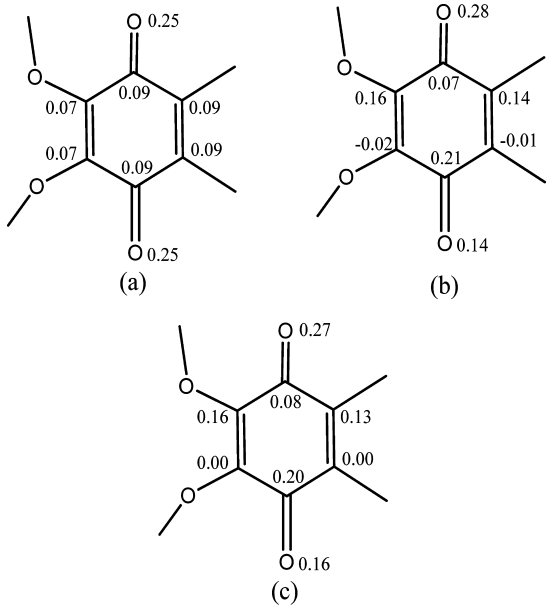

Figure 6. Mulliken spin populations for (a) isolated, (b) WT, and (c) D75H models. Atom numbering is as shown in Figure 1.

hyperfine couplings can be calculated and compared with available ^{15}N, ^{1}H, and ^{13}C experimental values. Table 4 lists the ^{15}N isotropic and anisotropic hyperfine couplings calculated for the WT and D75H models. In addition, the calculated ^{14}N qcc, K, and asymmetry parameters, η, are compared with experimental values. The experimental ^{15}N isotropic hyperfine couplings for N_ε and N_η of R71 (2.4 and 0.15 MHz, respectively), as well as K (0.93 MHz) and η (0.51) for N_ε of R71, are excellently reproduced by the WT model. For the H98 imidazole NH group, the calculations give an a_{iso} of 0.4 MHz, in reasonable agreement with the experimental value of 0.3 MHz. The value of the isotropic hyperfine couplings for these nitrogens is very sensitive to the angle made by the NH donor with respect to the SQ ring plane.[37] The very close correspondence between the calculated and experimental values for the WT model suggests that the orientation of these hydrogen bond donors in the optimized model is very similar to that adopted in the actual Q_H binding site.

For the D75H model, the optimized geometry gives rise to ^{15}N isotropic hyperfine couplings that deviate somewhat from the experimental determinations. N_ε of R71 has a calculated value of 1.4 MHz, whereas the experimental assignment is 0.6 MHz. The calculated value for the N_εH group of H75 is 0.8

Table 4. ^{15}N Isotropic, a_{iso}, and Anisotropic, T_{ii}, Hyperfine Tensors Calculated for the Q_H Site Models[a]

	WT				D75H			
position	$T_{zz}T_{yy}T_{xx}$	a_{iso}	K	η	$T_{zz}T_{yy}T_{xx}$	a_{iso}	K	η
R71 Nε	0.6 (0.9)	2.4 (2.4)	0.9 (0.9)	0.7 (0.5)	0.0	1.4, 0.5[b] (0.6)	0.9	0.8
	−0.3 (−0.6)				0.0			
	−0.3 (−0.3)				0.0			
R71 Nη	0.0	0.2 (0.15)	1.1	0.4	0.0	0.0 (0.0)	1.1	0.5
	0.0				0.0			
	0.0				0.0			
R71 Nη	0.0	0.0	1.2	0.2	0.0	0.0 (0.0)	1.2	0.3
	0.0				0.0			
	0.0				0.0			
H98 N	0.4	0.4 (0.3)	0.6	0.5	0.5	0.6 (0.8)	0.6	0.6
	−0.1				−0.2			
	−0.3				−0.3			
H75 N	–	–	–	–	0.4, 0.7[b] (0.9)	0.8, 2.5[b] (3.5)	0.5 (0.4)	0.6 (0.7)
					−0.2, −0.4[b] (−0.7)			
					−0.2, −0.3[b] (−0.2)			

[a]Calculated values for the ^{14}N nuclear quadrupole coupling constant (K) and the asymmetry parameter, η, are also given. Experimental values are given in parentheses. All values are in megahertz. [b]Values using adjusted orientation (see the text for details).

dx.doi.org/10.1021/bi300151q | *Biochemistry* 2012, 51, 3827−3838

Table 5. 5-Methyl- and Hydrogen-Bonded ^{1}H Isotropic, a_{iso}, and Anisotropic, T_{ii}, Hyperfine Tensors Calculated for the Q_H Site Model[a]

	isolated		WT		D75H	
position	$T_{zz}T_{yy}T_{xx}$	a_{iso}	$T_{zz}T_{yy}T_{xx}$	a_{iso}	$T_{zz}T_{yy}T_{xx}$	a_{iso}
5-CH_3	2.6	5.9 (6.0)	3.0	9.2 (9.5−10.0)	2.7	8.2 (8.0)
	−1.3		−1.5		−1.4	
	−1.3		−1.5		−1.4	
R71 NHε	–	–	8.6	−0.1	8.4	−0.2
			−4.1		−4.1	
			−4.5		−4.3	
R71 NHη	–	–	1.8	0.0	1.8	0.0
			−0.6		−0.6	
			−1.2		−1.2	
R71 NHη	–	–	0.8	0.0	0.8	0.0
			−0.3		−0.3	
			−0.5		−0.5	
H98 NH	–	–	8.2	−0.6	8.3	−0.7
			−3.9		−4.0	
			−4.2		−4.3	
D75/H75 COOH/NH	–	–	8.9	0.0	6.5	−0.4
			−4.4		−3.2	
			−4.5		−3.3	

[a]Experimental values are given in parentheses. All values are given in megahertz.

MHz, whereas the experimental assignment is 3.5 MHz. For the H98 imidazole group, the calculated value, 0.6 MHz, is in good agreement with the experimental assignment of 0.8 MHz. In the optimized D75H model, the imidazole NH group is oriented 42° out of the SQ ring plane. The sensitivity of the ^{15}N value to this orientation is demonstrated by changing the orientation of the NH group of H75 from the optimized value of 42° to 90°. This changes the calculated ^{15}N isotropic hyperfine coupling from 0.8 to 2.5 MHz, much closer to the experimentally measured value of 3.5 MHz. Likewise, changing the out-of-plane orientation of the guanidinium $N_\varepsilon H$ group from the optimized value of 41° to 35° changes the ^{15}N isotropic coupling from 1.4 to 0.6 MHz, in exact agreement with the experimental assignment. For the imidazole NH group of H75, the calculated ^{14}N qcc K has a value of 0.5 MHz and the asymmetry parameter, η, is calculated to be 0.6. These are in excellent agreement with our experimental determinations of 0.4 MHz and 0.7, respectively. Our conclusion, therefore, is that the D75H model is a good representation of the SQ_H in the mutant, but the orientation of the hydrogen bond donors is different from that of the optimized small model calculation.

Calculated hyperfine couplings can also be compared with previous experimental determinations of ^{1}H hyperfine couplings for the WT and D75H mutant. Rotating methyl groups are observed readily using ENDOR spectroscopy as they give a strong ENDOR response and have been used as a primary marker in gauging the spin density asymmetry within SQs in photosynthetic reaction centers.[38] The 5-CH_3 ^{1}H hyperfine coupling has been measured in numerous studies and indeed is the principal indicator that the spin density of the WT SQ_H is highly asymmetric compared with the radical generated in vitro. For the SQ in a nonpolar solvent and, therefore, not involved in hydrogen bonding, a_{iso} equals 6.0 MHz.[38] Our calculated value for the isolated model is 5.9 MHz, which is in excellent quantitative agreement with this determination. For our WT model of SQ_H, the calculated ^{1}H a_{iso} value is 9.2 MHz, which is in good accord with experimental values that vary from 9.5 to 10.0 MHz.[34] The elevated hyperfine coupling for the 5-CH_3 position is a result of the elevated spin population calculated for the ring C5 position shown in Figure 6. Previous DFT studies[33−35] using SQ anion models have been unable to match the experimental value for this position, and this can be mainly attributed to the use of water or amide groups as the hydrogen bonding groups in these modeling studies. Because the elevated 5-CH_3 hyperfine coupling was similar to that found for neutral semiquinone free radicals, it has been proposed that the Q_H site SQ is a neutral radical.[17,18] No evidence of formation of the neutral SQ form has been obtained with the current computational model, although this cannot be ruled out with a different larger model of the Q_H site. The asymmetry in spin density distribution for both scenarios is very similar. Our current computational studies indicate that the elevated 5-CH_3 coupling arises from strong hydrogen bonding of a semiquione anion radical to a positively charged guanidinium group and a carboxylic acid group, i.e., R71 and D75 in the WT SQ_H.

For the D75H model, the calculated 5-CH_3 isotropic hyperfine coupling of 8.2 MHz is lower than that of the WT model and is in excellent agreement with the value found experimentally for the D75H mutant of 8.0 MHz.[18] The lower value for this hyperfine coupling, compared to that of the WT, can be ascribed to the more symmetric spin density distribution for the D75H model compared with the WT (Figures 5 and 6). Replacement of the carboxylic acid group of D75 with the imidazole group of H75 results in significantly weaker hydrogen bonding to the O1 atom of the SQ_H. The more symmetric spin density distribution leads to a lower spin density at C5 and a lower ^{1}H hyperfine coupling value for the 5-CH_3 group compared with the WT model. The good reproduction of this well-characterized coupling suggests that the spin density distribution of the D75H model is reasonably accurate.

More recently, 2D ESEEM studies have yielded ^{13}C isotropic hyperfine coupling values for the 5-CH_3 carbon nucleus for both WT and D75H samples.[20] For the WT and D75H models, the calculated isotropic values of −5.3 and −4.4 MHz are in good agreement with the experimental values of −6.1 and −4.7 MHz, respectively.

dx.doi.org/10.1021/bi300151q | Biochemistry 2012, 51, 3827−3838

^{1}H hyperfine couplings have also been resolved from exchangeable, presumably hydrogen bonded, protons in both the WT and D75H mutant. Compared with methyl group hyperfine couplings, hydrogen-bonded protons are difficult to interpret in complex systems where there can be significant overlap of spectral lines. For the WT SQ_H, 2D ESEEM identified three protons having isotropic and anisotropic values (a_{iso} and T, respectively) of ∓0.7 and ±6.3 MHz, ∓1.2 and ±4.2 MHz, and ∓4.2 and ±1.7 MHz, respectively.[17] The calculated values of a_{iso} and $T = T_{zz}/2$ for the three hydrogen-bonded protons of D75, R71, and H98 are 0.0 and 4.5 MHz, −0.1 and 4.3 MHz, and −0.6 and 4.1 MHz, respectively (Table 5). The good agreement between the calculated R71 N_ε, ^{15}N a_{iso}, value and the experimental value indicates that the NH orientation relative to the SQ_H ring plane is accurately modeled for the WT. The most likely candidate for the strong H-bond observed experimentally is the COOH group of D75, which exhibits the shortest optimized hydrogen bond distance. In the optimized model of the WT, this is oriented 40° out of the ring plane. By changing this orientation to 90°, we calculate that the anisotropic coupling increases to 5.4 MHz with an isotropic coupling value of 0.8 MHz, which is in better agreement with the experimental values. Therefore, we assign the largest (−0.7, 6.3) MHz proton hyperfine coupling to the COOH proton of D75. The (−1.2, 4.2) MHz coupling could be due to an overlap of the H98 NH and R71 N_εH lines. None of our calculated values match the very unusual coupling of (∓4.2, ±1.7) MHz. The unusually large isotropic coupling together with the relatively small anisotropic component would suggest that this coupling does not arise from a hydrogen-bonded proton, and further experimental characterization is required.

For the D75H mutant, exchangeable protons have been experimentally assigned to ^{1}H hyperfine couplings (a_{iso} and T) of ∓1.0 and ±4.6 MHz and ∓4.3 and ±1.2 MHz, respectively. Three hydrogen bond donors are present in our D75H model: N_ε^{1}H of R71, N^{1}H of H75, and N^{1}H of H98 (Table 5). The calculated (a_{iso} and T) values of each of these are in reasonable agreement with the experimental values of 1.0 and 4.6 MHz, respectively, so all three may contribute to this experimentally determined coupling. As found with the WT model, the other experimentally observed coupling with a large isotropic and small anisotropic component, ∓4.3 and ±1.2 MHz, respectively, has no counterpart in the calculated values and is unlikely to be due to a proton(s) hydrogen bonded with carbonyls. One can suggest that exchangeable resonances with weaker *hfi* couplings observed in the spectra result from the overlap of the signals from the several protons in the SQ environment. Overlap of the cross-peak with different (but weak) hyperfine couplings would give cross-peaks with shapes and lengths substantially different from those of contributing signals. As a result, the analysis would give some "effective" couplings not related directly to the real values. We suggest that further experiments using fully deuterated protein and cofactor as well as HYSCORE and ENDOR experiments at Q-band will better resolve these couplings, which would identify their source. Q-Band will also address specific questions about the orientation of the H-bonds around the SQ_H site based on the hyperfine (and nuclear quadrupole) tensors of exchangeable protons (deuterons) that would lead to more adequate computational models.[39]

Relevance to the Quinone One-Electron Transfer Role. For in vitro systems, in protic solvents, quinone reduction or quinol oxidation proceeds via sequential loss or gain of two electrons via the semiquinone free radical form with consequent loss or gain of two protons. In biological systems, quinones can function additionally as one-electron transfer agents. For example, the Q_A site quinone in type II photosynthetic reaction centers acts as a one-electron transfer agent for transfer between a pheophytin molecule and the quinone reductase site Q_B.[28,38] In the photostsystem I reaction center, a phylloquinone molecule, A_1, also acts as a one-electron transfer agent for transfer between a chlorophyll molecule and an Fe_4S_4 center.[40,41] For Q_B, which undergoes two-electron reduction and subsequent protonation to the quinol, as in in vitro systems, a more symmetric spin density distribution is found.[38] The Q_B quinone is in dynamic equilibrium with a quinone pool and binds to receive two electrons and two protons before unbinding in the reduced quinol form. It is noteworthy that for the quinones functioning as one-electron transfer agents, an extremely asymmetric spin density distribution has been found for the SQ form, whereas in a true substrate binding quinone site, such as Q_B, a more symmetric spin density has been found, i.e., similar to that found in protic solvents. To fulfill the role of a one-electron transfer agent, it may be a requirement of the quinone binding site to produce a highly asymmetric spin density distribution for the SQ intermediate. The asymmetry in the spin density distribution for the semiquinone reflects a more contracted/localized electron density distribution for the singly occupied molecular orbital, SOMO, of the free radical anion. This is clearly shown by the spin density contours in Figure 5. This contracted electron density distribution would be expected to lead to a less stable SQ form compared with the symmetrical form but would also imply that further one-electron reduction to the two-electron reduced dianion or quinol form would be unfavorable as now two electrons have to occupy the contracted asymmetric orbital. While the exact mechanism of electron transfer and reduction at the Q_H site is still unknown, it is believed to shuttle electrons from a true quinone substrate binding site Q_L to heme *b* for the eventual reduction of oxygen at the heme o_3−Cu_B active site.[7,13] It would appear to perform a function similar to that if the Cu_A site in cytochrome *c* oxidase. As for the Q_A and A_1 quinones described above, the high asymmetry in spin density distribution observed for SQ_H would indicate that it performs a similar one-electron transfer role and that high asymmetry in the SOMO electron density distribution may be a crucial factor in determining the quinone role as an effective one-electron transfer agent. In this study, therefore, one possibility for the nonactivity exhibited by the D75H mutant could be related to the more symmetrical spin density distribution of the Q_H site SQ compared with the WT. The asymmetry in spin density distribution is still quite large however for the D75H mutant, compared to the symmetrical situation. This would argue against the hypothesis given above, unless rapid one-electron transfer requires the extreme asymmetry that is present in the WT sample and also present in the Q_A and A_1 sites.

■ CONCLUSIONS

In this study, the pulsed EPR experiments performed with the selectively ^{15}N labeled cyt bo_3 samples have led to the unambiguous assignment of N_ε of R71 as the nitrogen that is strongly coupled to the Q_H site SQ in the wild-type enzyme and gives rise to the observed ^{14}N ESEEM signals. In addition, selective ^{15}N labeling of cyt bo_3 has allowed the detection of even weak interactions between the SQ_H and individual

residues at the ubiquinone binding site as summarized in Table 2. The HYSCORE data suggest that H98 at the Q_H site is weakly coupled to the semiquinone radical and there is no direct interaction between the SQ_H and N_ε of Q101. The ^{15}N selective labeling has also identified N_ε of H75 as the nitrogen hydrogen bonded with the SQ_H of the D75H mutant enzyme.

Density functional calculations on models of the active site for both the WT and D75H systems show good agreement between experimentally observed and calculated values of available $^{14,15}N$, ^{1}H, and ^{13}C couplings. The model studies indicate that a very strong hydrogen bonding interaction occurs between the O1 atom of the SQ_H and the hydrogen bond donor groups of R71 and D75 with a relatively weaker interaction occurring for O4 and the imidazole NH group of H98. This is mainly responsible for the highly asymmetric spin density distribution observed experimentally. Replacement of D75 with H75 in the D75H mutant model leads to a lower spin density asymmetry for the SQ_H. The HYSCORE results also imply that in the D75H mutant, N_ε of R71 possesses significantly smaller hyperfine coupling than that in the WT protein despite practically the same length of the H−O bond in the optimized structure. This suggests that the orientation of the hydrogen bond donors is different from that of the optimized small model calculation for D75H. On the basis of previous studies of quinone one-electron transfer sites, we further postulate that the highly asymmetric spin density distribution of the WT SQ_H may be a significant factor in its role as a one-electron transfer agent for transfer between the substrate binding site and heme *b*.

Overall, our combined pulsed EPR experiments and electronic structure calculations constitute a major step toward complete characterization of the distribution of the unpaired spin density of the SQ in the Q_H site. The interactions between the SQ and nearby residues unraveled in this study are crucial for understanding how the radical is stabilized inside the protein's binding pocket and establish a foundation for future studies of quinone structure−function relationships in bioenergetics.

■ ASSOCIATED CONTENT

Supporting Information

Model of the Q_H site, ^{14}N and ^{15}N three-pulse and HYSCORE spectra of the Q_H site SQ in WT and D75H cyt bo_3, structures of amino acids selectively labeled in this work showing the atomic numbering, and the complete ref 27. This material is available free of charge via the Internet at http://pubs.acs.org.

■ AUTHOR INFORMATION

Corresponding Author

*S.A.D.: e-mail, dikanov@illinois.edu; phone, (217) 244-1186. R.B.G.: e-mail, r-gennis@illinois.edu; phone, (217) 333-9075. P.J.O.: e-mail, patrick.o'malley@manchester.ac.uk; phone, +44 161 306 4536.

Present Address

[@]Department of Molecular Biology and Genetics, 321 Biotechnology Building, Cornell University, Ithaca, NY 14853.

Funding

This investigation was supported by Grants DE-FG02-08ER15960 (S.A.D.) and DE-FG02-87ER13716 (R.B.G.) from the Chemical Sciences, Geosciences and Biosciences Division, Office of Basic Energy Sciences, Office of Sciences, U.S. Department of Energy, National Institutes of Health Grant GM062954 (S.A.D.), and National Center for Research Resources Grants S10-RR015878 and S10-RR025438 for instrumentation.

Notes

The authors declare no competing financial interest.

■ ACKNOWLEDGMENTS

P.J.O. acknowledges the use of the EPSRC UK National Service for Computational Chemistry Software (NSCCS) in carrying out this work.

■ ABBREVIATIONS

2D, two-dimensional; CW EPR, continuous wave electron paramagnetic resonance; cyt bo_3, cytochrome bo_3 ubiquinol oxidase from *E. coli*; DDM, *n*-dodecyl β-D-maltoside; DFT, density functional theory; ESEEM, electron spin echo envelope modulation; HYSCORE, hyperfine sublevel correlation; nqi, nuclear quadrupole interactions; $\mathbf{N}_{wc}$, weakly coupled nitrogens; qcc, quadrupole coupling constant; Q_H, high-affinity quinone-binding site; Q_L, low-affinity quinone-binding site; SQ, semiquinone; SQ_H, semiquinone at the Q_H site; UQ_8, ubiquinone-8; WT, wild-type.

■ REFERENCES

(1) Anraku, Y. (1988) Bacterial electron transport chains. *Annu. Rev. Biochem. 57*, 101−132.

(2) Puustinen, A., Finel, M., Virkki, M., and Wikstrom, M. (1989) Cytochrome o (bo) is a proton pump in *Paracoccus denitrificans* and *Escherichia coli*. *FEBS Lett. 249*, 163−167.

(3) Puustinen, A., Finel, M., Haltia, T., Gennis, R. B., and Wikstrom, M. (1991) Properties of the two terminal oxidases of *Escherichia coli*. *Biochemistry 30*, 3936−3942.

(4) Garcia-Horsman, J. A., Barquera, B., Rumbley, J., Ma, J., and Gennis, R. B. (1994) The superfamily of heme-copper respiratory oxidases. *J. Bacteriol. 176*, 5587−5600.

(5) Trumpower, B. L., and Gennis, R. B. (1994) Energy transduction by cytochrome complexes in mitochondrial and bacterial respiration: The enzymology of coupling electron transfer reactions to transmembrane proton translocation. *Annu. Rev. Biochem. 63*, 675−716.

(6) Puustinen, A., Verkhovsky, M. I., Morgan, J. E., Belevich, N. P., and Wikstrom, M. (1996) Reaction of the *Escherichia coli* quinol oxidase cytochrome bo_3 with dioxygen: The role of a bound ubiquinone molecule. *Proc. Natl. Acad. Sci. U.S.A. 93*, 1545−1548.

(7) Yap, L. L., Lin, M. T., Ouyang, H., Samoilova, R. I., Dikanov, S. A., and Gennis, R. B. (2010) The quinone-binding sites of the cytochrome bo_3 ubiquinol oxidase from *Escherichia coli*. *Biochim. Biophys. Acta 1797*, 1924−1932.

(8) Sato-Watanabe, M., Mogi, T., Ogura, T., Kitagawa, T., Miyoshi, H., Iwamura, H., and Anraku, Y. (1994) Identification of a novel quinone-binding site in the cytochrome *bo* complex from *Escherichia coli*. *J. Biol. Chem. 269*, 28908−28912.

(9) Sato-Watanabe, M., Itoh, S., Mogi, T., Matsuura, K., Miyoshi, H., and Anraku, Y. (1995) Stabilization of a semiquinone radical at the high-affinity quinone-binding site (Q_H) of the *Escherichia coli bo*-type ubiquinol oxidase. *FEBS Lett. 374*, 265−269.

(10) Ingledew, W. J., Ohnishi, T., and Salerno, J. C. (1995) Studies on a stabilisation of ubisemiquinone by *Escherichia coli* quinol oxidase, cytochrome *bo*. *Eur. J. Biochem. 227*, 903−908.

(11) Sato-Watanabe, M., Mogi, T., Miyoshi, H., and Anraku, Y. (1998) Characterization and functional role of the Q_H site of *bo*-type ubiquinol oxidase from *Escherichia coli*. *Biochemistry 37*, 5356−5361.

(12) Mogi, T., Sato-Watanabe, M., Miyoshi, H., and Orii, Y. (1999) Role of a bound ubiquinone on reactions of the *Escherichia coli* cytochrome *bo* with ubiquinol and dioxygen. *FEBS Lett. 457*, 223−226.

(13) Kobayashi, K., Tagawa, S., and Mogi, T. (2000) Transient formation of ubisemiquinone radical and subsequent electron transfer

process in the *Escherichia coli* cytochrome *bo*. *Biochemistry 39*, 15620−15625.
(14) Abramson, J., Riistama, S., Larsson, G., Jasaitis, A., Svensson-Ek, M., Laakkonen, L., Puustinen, A., Iwata, S., and Wikstrom, M. (2000) The structure of the ubiquinol oxidase from *Escherichia coli* and its ubiquinone binding site. *Nat. Struct. Biol. 7*, 910−917.
(15) Hellwig, P., Yano, T., Ohnishi, T., and Gennis, R. B. (2002) Identification of the residues involved in stabilization of the semiquinone radical in the high-affinity ubiquinone binding site in cytochrome bo_3 from *Escherichia coli* by site-directed mutagenesis and EPR spectroscopy. *Biochemistry 41*, 10675−10679.
(16) Grimaldi, S., MacMillan, F., Ostermann, T., Ludwig, B., Michel, H., and Prisner, T. (2001) $Q_H{}^{*-}$ ubisemiquinone radical in the bo_3-type ubiquinol oxidase studied by pulsed electron paramagnetic resonance and hyperfine sublevel correlation spectroscopy. *Biochemistry 40*, 1037−1043.
(17) Yap, L. L., Samoilova, R. I., Gennis, R. B., and Dikanov, S. A. (2006) Characterization of the exchangeable protons in the immediate vicinity of the semiquinone radical at the Q_H site of the cytochrome bo_3 from *Escherichia coli*. *J. Biol. Chem. 281*, 16879−16887.
(18) Yap, L. L., Samoilova, R. I., Gennis, R. B., and Dikanov, S. A. (2007) Characterization of mutants that change the hydrogen bonding of the semiquinone radical at the Q_H site of the cytochrome bo_3 from *Escherichia coli*. *J. Biol. Chem. 282*, 8777−8785.
(19) Lin, M. T., Samoilova, R. I., Gennis, R. B., and Dikanov, S. A. (2008) Identification of the nitrogen donor hydrogen bonded with the semiquinone at the Q_H site of the cytochrome bo_3 from *Escherichia coli*. *J. Am. Chem. Soc. 130*, 15768−15769.
(20) Lin, M. T., Shubin, A. A., Samoilova, R. I., Narasimhulu, K. V., Baldansuren, A., Gennis, R. B., and Dikanov, S. A. (2011) Exploring by pulsed EPR the electronic structure of ubisemiquinone bound at the Q_H site of cytochrome bo_3 from *Escherichia coli* with in vivo ^{13}C-labeled methyl and methoxy substituents. *J. Biol. Chem. 286*, 10105−10114.
(21) Datsenko, K. A., and Wanner, B. L. (2000) One-step inactivation of chromosomal genes in *Escherichia coli* K-12 using PCR products. *Proc. Natl. Acad. Sci. U.S.A. 97*, 6640−6645.
(22) Epel, B., and Silakov, A. *KAZAN viewer for Matlab: Visualisation and data processing GUI for EPR and NMR*, 2007, http://www.boep.specman4epr.com/kv_intro.html.
(23) Martin, E., Samoilova, R. I., Narasimhulu, K. V., Wraight, C. A., and Dikanov, S. A. (2010) Hydrogen bonds between nitrogen donors and the semiquinone in the Q_B site of bacterial reaction centers. *J. Am. Chem. Soc. 132*, 11671−11677.
(24) Höfer, P., Grupp, A., Nebenführ, H., and Mehring, M. (1986) Hyperfine sublevel correlation (hyscore) spectroscopy: A 2D ESR investigation of the squaric acid radical. *Chem. Phys. Lett. 132*, 279−282.
(25) Dikanov, S. A., and Bowman, M. K. (1995) Cross-peak lineshape of two-dimensional ESEEM spectra in disordered S = 1/2, I = 1/2 spin systems. *J. Magn. Reson., Ser. A 116*, 125−128.
(26) Dikanov, S. A., Tyryshkin, A. M., and Bowman, M. K. (2000) Intensity of cross-peaks in HYSCORE spectra of $S = 1/2$, $I = 1/2$ spin systems. *J. Magn. Reson. 144*, 228−242.
(27) Frisch, M. J., et al. (2009) *Gaussian 09*, Gaussian, Inc., Wallingford, CT.
(28) Lin, T.-J., and O'Malley, P. J. (2011) An ONIOM study of the spin density distribution of the Q_A site plastosemiquinone in the photosystem II reaction center. *J. Phys. Chem. B 115*, 4227−4233.
(29) Martin, E., Samoilova, R. I., Narasimhulu, K. V., Lin, T. J., O'Malley, P. J., Wraight, C. A., and Dikanov, S. A. (2011) Hydrogen bonding and spin density distribution in the Q_B semiquinone of bacterial reaction centers and comparison with the Q_A site. *J. Am. Chem. Soc. 133*, 5525−5537.
(30) Dikanov, S. A., Samoilova, R. I., Kappl, R., Crofts, A. R., and Hüttermann, J. (2009) The reduced [2Fe-2S] clusters in adrenodoxin and *Arthrospira platensis* ferredoxin share spin density with protein nitrogens, probed using 2D ESEEM. *Phys. Chem. Chem. Phys. 11*, 6807−6819.
(31) Dikanov, S. A., Shubin, A. A., Kounosu, A., Iwasaki, T., and Samoilova, R. I. (2004) A comparative, two-dimensional ^{14}N ESEEM characterization of reduced [2Fe-2S] clusters in hyperthermophilic archaeal high- and low-potential Rieske-type proteins. *J. Biol. Inorg. Chem. 9*, 753−767.
(32) Iwasaki, T., Kounosu, A., Uzawa, T., Samoilova, R. I., and Dikanov, S. A. (2004) Orientation-selected ^{15}N-HYSCORE detection of weakly coupled nitrogens around the archaeal Rieske [2Fe−2S] center. *J. Am. Chem. Soc. 126*, 13902−13903.
(33) Boesch, S. E., and Wheeler, R. A. (2009) Isotropic ^{13}C hyperfine coupling constants distinguish neutral from anionic ubiquinone-derived radicals. *ChemPhysChem 10*, 3187−3189.
(34) Kacprzak, S., Kaupp, M., and MacMillan, F. (2006) Protein−cofactor interactions and EPR parameters for the Q_H quinone binding site of quinol oxidase. A density functional study. *J. Am. Chem. Soc. 128*, 5659−5671.
(35) MacMillan, F., Kacprzak, S., Hellwig, P., Grimaldi, S., Michel, H., and Kaupp, M. (2011) Elucidating mechanisms in haem copper oxidases: The high-affinity Q_H binding site in quinol oxidase as studied by DONUT-HYSCORE spectroscopy and density functional theory. *Faraday Discuss. 148*, 315−344.
(36) O'Malley, P. J. (1997) Effect of hydrogen bonding on the spin density distribution and hyperfine couplings of the p-benzosemiquinone anion radical in alcohol solvents: A hybrid density functional study. *J. Phys. Chem. A 101*, 9813−9817.
(37) O'Malley, P. J. (1998) A density functional study of the effect of orientation of hydrogen bond donation on the hyperfine couplings of benzosemiquinones: Relevance to semiquinone-protein hydrogen bonding interactions in vivo. *Chem. Phys. Lett. 291*, 367−374.
(38) Lubitz, W., and Feher, G. (1999) The primary and secondary accepters in bacterial photosynthesis III. Characterization of the quinone radicals $Q_A{}^{-\bullet}$ and $Q_B{}^{-\bullet}$ by EPR and ENDOR. *Appl. Magn. Reson. 17*, 1−48.
(39) Flores, M., Isaacson, R., Abresch, E., Calvo, R., Lubitz, W., and Feher, G. (2007) Protein-cofactor interactions in bacterial reaction centers from *Rhodobacter sphaeroides* R-26: II. Geometry of the hydrogen bonds to the primary quinone $Q_A{}^{\bullet-}$ by ^1H and ^2H ENDOR spectroscopy. *Biophys. J. 92*, 671−682.
(40) Lin, T.-J., and O'Malley, P. J. (2011) Binding site influence on the electronic structure and electron paramagnetic resonance properties of the phyllosemiquinone free radical of photosystem I. *J. Phys. Chem. B 115*, 9311−9319.
(41) Srinivasan, N., and Golbeck, J. H. (2009) Protein-cofactor interactions in bioenergetic complexes: The role of the A_{1A} and A_{1B} phylloquinones in Photosystem I. *Biochim. Biophys. Acta 1787*, 1057−1088.